

Thermal-wave infrared radiometric slice diffraction tomography with back-scattering and transmission reconstructions: experimental

Lena Nicolaides, Mahendra Munidasa and Andreas Mandelis

Photothermal and Optoelectronic Diagnostics Laboratories, Department of Mechanical Engineering, University of Toronto, and Manufacturing Research Corporation of Ontario (MRCO), 5 King's College Road, Toronto, Ontario, Canada M5S 3G8

Received 5 August 1996, in final form 18 July 1997

Abstract. Laser infrared photothermal radiometry is developed into a thermal-wave slice diffraction tomography (TSDT) instrumentation and measurement methodology for cross sectional imaging of subsurface defects. A mild-steel sample with artificial subsurface defects is used to test the TSDT potential. Experimental reconstructions using the Born approximation both in back-scattering and transmission modes are presented. The numerically reconstructed experimental data constitute the first experimental TSD tomograms, which were found to be limited by instrumental aperture-broadening effects.

1. Introduction

An improved experimental, quantitative/computational thermal-wave slice diffraction tomography (TSDT) technology over an earlier version [1] is developed as a complementary tool (in terms of depth-probing ranges) to acoustic and ultrasonic tomography, but for entirely different geometries and more general classes of materials, processes and manufacturing parameters. This differentiation of TSDT from the other tomographic technologies is partly based on the fact that the imaged quantity is the cross sectional thermal diffusivity, instead of ultrasonic velocity for instance. Unlike electromagnetic or acoustic tomography, thermal-wave tomography features: (a) short propagation distances of the thermal wave, (b) a complex thermal wavevector lying along the 45° line in the complex plane [2], (c) non-rotational access to the sample in most practical situations [1]. Therefore, the conventional reconstruction of the well posed propagating wave-field tomographies [3] cannot be applied in the case of the thermal-wave problem. A mathematical model that represents the behaviour of three-dimensional thermal waves has been developed [4] and evaluated with a numerical reconstruction technique [5].

Experimentally the technique is made truly non-contact by obtaining cross sectional scans through infrared photothermal radiometric detection. A focused laser beam and an emitted black-body radiation detector are scanned across a material cross section and the photothermal radiometric signal is recorded in back scatter or transmission at each relative laser position. Scans on a mild-steel sample, with machined subsurface defects, were made to test the ability and performance of TSDT. The scanned thermal-wave data, for one point source and multiple detection points, were used as an input to reconstruct the cross sectional slice thermal diffusivity image. A final reconstruction was formed by averaging

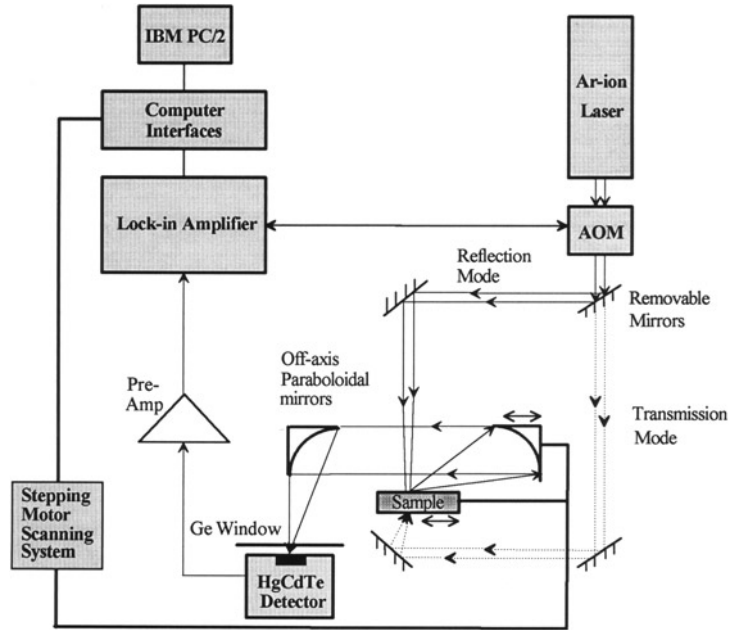


Figure 1. Schematic diagram of the experimental set-up capable of both reflection and transmission mode TSDT.

over reconstructions of several source positions. The numerically reconstructed experimental data constitute the first reported experimental TSDT.

2. Experimental method and data

The experimental technique best suited to acquire the scanned data for TSDT was explored. The data were obtained at one cross section from different laser and detector positions. Historically, the first detection method used to obtain tomographic slice data was photopyroelectric detection [1, 6], which was limited to transmission measurements. The current experimental method, based on photothermal radiometric detection, has the flexibility for both back-scattering and transmission measurements in a truly non-contact manner.

2.1. Experimental system

The experimental set-up for cross sectional imaging via photothermal radiometric detection is shown in figure 1. A 514.5 nm wavelength CW Innova 100 Ar⁺ laser from Coherent is modulated at frequency $f = \omega/2\pi$, where ω is the angular modulation frequency, and then focused onto a sample to a spot size of approximately 50 μm in transmission mode or 35 μm in back-scattering mode, at an output power of 2 W. The modulation is performed by an external acousto-optic modulator (AOM, ISOMET 1201E-1). The black-body radiation from the optically excited sample is collected and collimated by two off-axis paraboloidal mirrors and then focused onto a liquid-nitrogen-cooled mercury-cadmium-telluride (HgCdTe) detector (EG & G Judson Model J15D12-M204-S050U). The heated area of the sample is centred around the focal point of one mirror, and the detector is at

the focal point of the other mirror. The sample and mirror 1 are mounted on separate micrometer stages driven by stepping motors controlled by a personal computer as shown symbolically by \leftrightarrow in figure 1. The HgCdTe detector is a photoconductive element, which undergoes a change in resistance proportional to the intensity of the incident infrared radiation. It has an active square size area of $50 \mu\text{m} \times 50 \mu\text{m}$ and a spectral bandwidth of $2\text{--}12 \mu\text{m}$. Its efficiency increases with decreasing temperature, so the detector is operated at a cryogenic temperature of 77 K. An anti-reflection (A-R) coated germanium window with a transmission bandwidth of $2\text{--}14 \mu\text{m}$ is mounted in front of the detector to block any visible radiation from the pump laser. The photothermal radiometric signal is amplified by a preamplifier with a frequency bandwidth dc-1 MHz (EG & G Judson Model PA-300), especially designed for operation with the HgCdTe detector, before being sent to the digital lock-in amplifier (Stanford Research System Model SR850). The low-noise preamplifier ensures proper performance for subsequent signal processing with a lock-in amplifier. The lock-in amplifier, which is interfaced with a personal computer, receives the pre-amplifier output. This process of data acquisition, storage, and scanning is fully automated. The instrumentation has the ability to perform in either back-scattering or transmission mode by directing the laser beam to the front or rear surface of the sample using removable mirrors.

Cross sectional imaging refers to a line scan that will obtain information about the sample cross section normal to its surface plane [1, 7]. The experimental information is used to reconstruct the respective cross sectional slice. In the experimental set-up, both the modulated heat source and the detector are localized, and therefore can be scanned independently. Moving the sample becomes equivalent to moving the laser beam, and moving mirror 1 becomes equivalent to moving the detector (figure 1). For each laser position, data are collected at several detector positions along a straight line. This defines the cross sectional plane to be imaged (PQSR plane, figure 2). The scan is repeated for different laser positions.

A circular mild-steel alloy with two subsurface defects was used for the experiments. Steel has a good thermal emissivity and non-machined pieces of it can be taken as a homogeneous sample in order to test the reconstruction technique. Figure 3 shows a mild-steel sample, with thickness 2 mm and diameter 15 mm. It contains two subsurface holes of diameter 0.635 and 0.8 mm at different depths. One hole is located 0.1 mm below the surface and the other hole is 0.6 mm below the surface.

2.2. Experimental data

Experiments were performed in both back-scattering and transmission mode with the mild-steel sample shown in figure 3. One experiment was performed in back scattering with the defect close to the front surface, and three experiments were performed in transmission with the defects at different depths. In all of the four experiments performed, a 3 mm scan was examined with the hole placed at the centre of the scan. Lines AB and CD in figure 3 are examples of line scans performed on the sample. The exact x -position of the defect in the

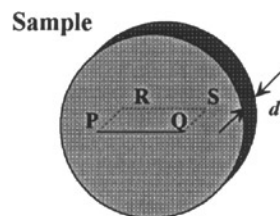


Figure 2. Line scan of a sample of thickness d for cross sectional imaging.

line scan was obtained by performing a conventional projectional scan, which is achieved by scanning the laser and the detector together.

Experiment number 1 was performed in back scattering at a modulation frequency $f = 15$ Hz, along cross section AB, with the defect near the front surface of the sample in figure 3. The thermal diffusion length at this frequency is 0.48 mm. The defect imaged was a shallow hole, 0.1 mm from the front surface of the sample and 0.635 mm in diameter. Figure 4 shows a conventional projectional scan along line AB. The amplitude of the scan exhibits a maximum at the defect location, whereas the phase is a minimum. The amplitude of the signal is influenced by surface blemishes, whereas the phase is unaffected, and, thus, truly represents subsurface defects [8]. From the scan data the defect is found to be at the centre of the scan ($x = 1.5$ mm). Figure 5 is (a) the amplitude and (b) the phase of the back-scattering cross sectional imaging data from five laser positions. For the tomographic

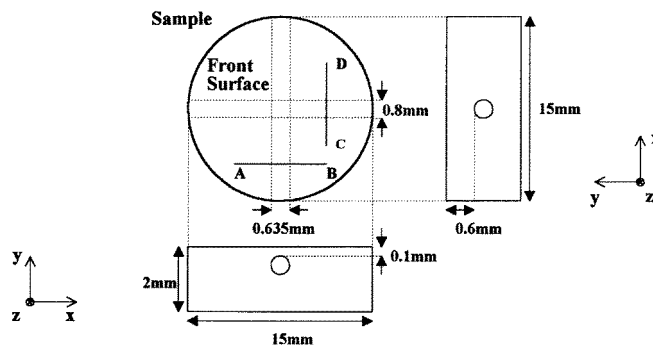


Figure 3. Mild-steel sample geometry.

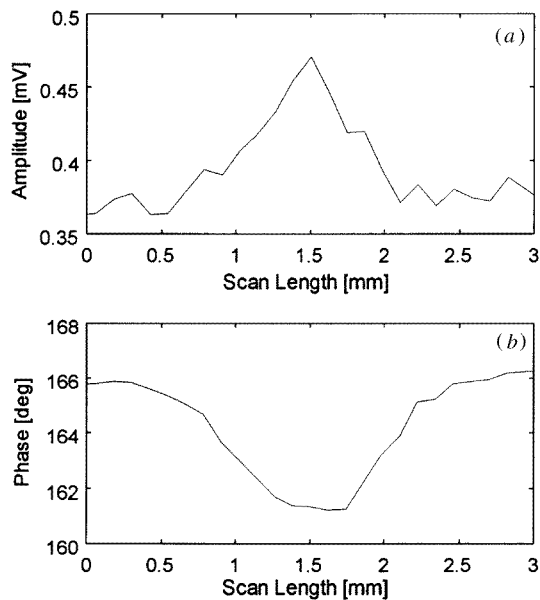


Figure 4. A back-scattering projectional scan. A conventional photothermal scan along line AB, front surface of sample, obtained at $f = 15$ Hz. (a) Signal amplitude, (b) signal phase.

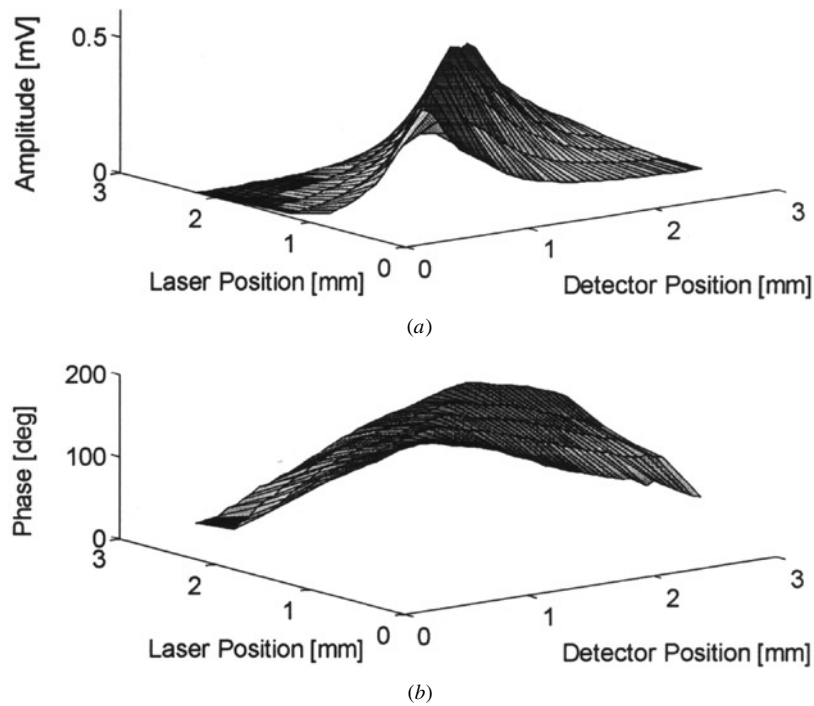


Figure 5. A back-scattering cross sectional imaging—shallow defect. Cross sectional image of five laser positions with 49 detector points. (a) Amplitude and (b) phase data at $f = 15$ Hz, obtained from a line scan of length 3 mm, represented in figure 4.

images, minimum requirements are both amplitude and phase from one laser position. Five 3 mm scans were performed along line AB at 49 detector points. The laser positions used were $x_{1(\text{laser})} = 0.8, 1.2, 1.5, 1.8, 2.2$ mm, where $x_{1(\text{laser})}$ is the coordinate at the front surface of the cross sectional region. Since this was a back-scattering experiment, detection occurred at the front surface of the sample with the laser source at the front surface.

The information given from a projectional scan is also included in a cross sectional image created by detecting a scan at different laser positions: the maximum of the signal always occurs when the laser and the detector are aligned with each other. The maximum lateral displacement of the laser position defines the extent of the scan. The diagonal line in the experimental data, in figure 5, defined between points (0, 0) and (3, 3), is equivalent to a projectional scan. It was verified that in figure 5(a) the diagonal five points create a maximum for amplitude data equivalent to the projectional scan in figure 4(a) and a minimum for the phase data in figure 5(b), equivalent to figure 4(b). Scanning of more laser positions for the cross sectional image would display the defect location along the scan direction more clearly; therefore a projectional scan would not be needed.

Experiment number 2 was performed in transmission mode with the same sample geometry as the previous experiment in figure 5, with the defect 0.1 mm deep into the material (shallow hole). A transmission projectional scan, at a modulation frequency of 15 Hz, of cross section AB (figure 3) at the front of the sample with a thermal diffusion length of 0.56 mm, was performed. Both amplitude and phase of the scan exhibited a minimum where the defect was located. The defect location was at the centre of the scan ($x = 1.5$ mm). The cross sectional imaging data were then collected at five laser positions,

$x_1 = 0, 0.75, 1.5, 2.25,$ and 3 mm.

A transmission projectional scan, at a modulation frequency of 11 Hz, of cross section CD (figure 3) with the defect closer to the front of the sample, was performed (middle hole—*experiment number 3*). The diameter of the defect was 0.8 mm and the depth was 0.6 mm from the front surface. Both the amplitude and the phase of the scan showed a minimum. The defect was located at $x = 1.4$ mm. The transmission cross sectional imaging experiment at five laser positions, $x_1 = 0, 0.75, 1.5, 2.5,$ and 3 mm, was subsequently performed.

Finally, a transmission projectional scan, at modulation frequency of 11 Hz, of cross section AB (figure 3), with the defect near the back surface of the sample was performed (deep hole—*experiment number 4*). This is the flipped geometry of experiment 2 and is defined as a defect which was 1.265 mm deep into the material from the front surface. Both amplitude and phase had a minimum at the location of the defect. The defect was located at the centre of the scan. The amplitude- and phase-transmission cross sectional imaging data were gathered at five laser positions, $x_1 = 0, 0.75, 1.5, 2.25,$ and 3 mm.

3. Tomographic inversions

Tomographic reconstructions from the foregoing experimental data were carried out. The reconstructions were produced by use of the Born approximation, with a computational methodology utilizing the Tikhonov regularization method adapted to the thermal-wave problem [5].

3.1. Reconstruction method

In reconstructing an image, the minimum requirement is one set of experimental data, represented by one laser position and multiple detector points. Both amplitude and phase are used to describe the total surface field. The reconstructed object function, $F(\mathbf{r})$, is the following non-dimensional function [2],

$$F(\mathbf{r}) \equiv n^2(\mathbf{r}) - 1 \quad (1)$$

where $n(\mathbf{r})$ is the ratio of the thermal diffusivity of the background, α_0 , to that of the defect, $\alpha(\mathbf{r})$, defined by:

$$n(\mathbf{r}) = \sqrt{\frac{\alpha_0}{\alpha(\mathbf{r})}}. \quad (2)$$

This ratio is a measure of the variation of the values of the thermal diffusivity in the scattering object from that of the surrounding region. The object function, $F(\mathbf{r})$, is a real number with a zero imaginary part [9, 10]. In all the reconstructions performed, the imaginary part was less than 10% of the magnitude of the object function. This served as a condition for choosing the correct regularization parameter needed for the Tikhonov reconstruction method. To solve for the object function, $F(\mathbf{r})$, the following linear system was formed,

$$(\sigma \mathbf{I} + \mathbf{A}^* \mathbf{A}) \mathbf{x} = \mathbf{A}^* \mathbf{b} \quad (3)$$

where σ is the Tikhonov regularization parameter, \mathbf{b} matrix is the experimental scattering field and \mathbf{A} is the theoretical ill-conditioned matrix representing the three-dimensional thermal-wave Green's function [4] times the homogeneous field [5]; the starred quantities denote adjoint matrices. An optimal solution to the linear system (3) was given by the regularization parameter, σ , that produced an object function with an imaginary part

of approximately zero. The background thermal diffusivity, α_0 , thermal conductivity, k , modulation frequency, f , and laser beam size, w , are necessary parameters for the calculation of the homogeneous thermal-wave field. For the thermal-diffusivity measurement of steel the experimental set-up in figure 1 was used by directing the pump laser onto the back surface of the sample and measuring the IR radiometric emission from the opposite surface. The theory given in [11] was fitted to the experimental data to obtain the thermal diffusivity, α and the thermal conductivity, k , was then calculated by $k = \rho c \alpha$ where ρ is the mass density and c is the specific heat. The input parameters for the inversion technique were $\alpha_{\text{steel}} = 1.1 \times 10^{-5} \text{ m}^2 \text{ s}^{-1}$ and $k_{\text{steel}} = 45 \text{ W m}^{-1} \text{ K}^{-1}$. The expected maximum magnitude of the non-dimensional object function, with a thermal diffusivity for the defect of $\alpha_{\text{air}} = 2.2 \times 10^{-5} \text{ m}^2 \text{ s}^{-1}$, was -0.5 . Experimentally, the total surface field data, measured at 49 detector positions, were interpolated to the desired number of points for a square matrix, using the cubic-splines interpolation technique. All reconstructions were computed for a grid size of $n = 10$, so that the linear system consisted of 100 equations with 100 unknowns.

3.2. Tomograms

The first reconstruction attempted was of the back-scattering experiment number 1 (figure 5), of the shallow hole. Figure 6 is the average reconstruction of five laser-position reconstructions obtained individually from the experimental data. The individual numerical reconstructions were performed with the laser position at $x_1 = 0.8, 1.2, 1.5, 1.8$ and 2.2 mm and the experimental amplitude and phase data of the respective laser position were used as input parameters for the inversion technique. The experimental data represented the

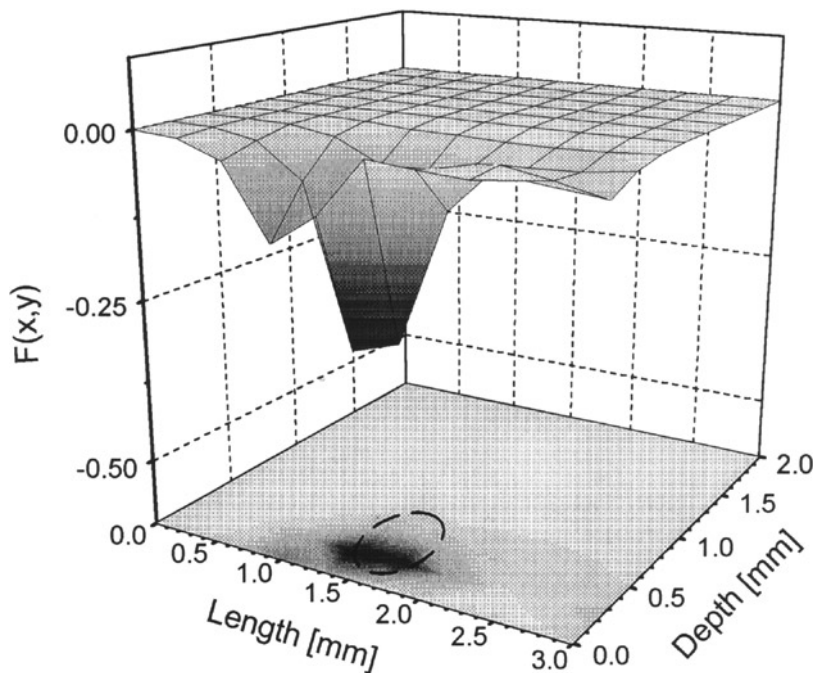


Figure 6. The inverse process-TSDT back-scattering reconstruction of the shallow defect. An average of five laser positions (true defect shown by the broken circle).

total surface thermal-wave field of the cross section imaged. Figure 6 reconstructs the object function $F(x, y)$, with a filled isometric contour of the reconstruction function at the bottom. The broken circle on the isometric contour of figure 6 shows the location and size of the true defect. The overall contrast of the reconstruction is -0.4 as compared with the expected magnitude of -0.5 . In averaging, information was lost due to the fact that a few reconstructions underestimated the defect magnitude; the use of more laser positions for averaging reconstructions would ensure accuracy for the magnitude of the object function. The location of the defect is very accurate but its size is broadened in the x -direction and diminished in the y -direction. The size of the defect as seen from the front surface is precise but the back of the defect is degraded, as expected from the theoretical simulations of [5]. Although the true defect edge is 0.6 mm deep, it is only reconstructed up to, approximately, 0.5 mm. This can be attributed to the fact that, in back-scattering mode, the thermal wave travels twice the defect depth for the scatterer to be seen. Beyond a total distance of two thermal diffusion lengths, information is lost [8]. All individual laser-position reconstructions of the experiment in figure 5 used the same regularization parameter of 10^{-4} , implying that this is an ill-defined problem that can give a reasonable solution after being regularized. Averaging seems to be very efficient in producing a good reconstruction since any artefacts created by individual reconstructions, especially around the laser-source location, are diminished. The back-scattering reconstruction shown in figure 6 is a good reconstruction and proves the validity of the reconstruction method. In summary, from individual reconstructions it was found that precise delineation of the defect occurs mostly on the side closer to the laser position and that only limited information is obtained through one laser-position reconstruction. Thus information obtained from multiple laser positions can create a satisfactory reconstruction when all reconstructions are combined by averaging.

The next reconstruction was of the transmission experiment number 2 (shallow hole). Figure 7 is the average reconstruction of five laser positions at $x_1 = 0, 0.75, 1.5, 2.25$ and 3 mm. The contrast is more satisfactory than that of the individual reconstructions. The defect is shown clearly and any artefacts at the back surface of the sample from the particular reconstructions are attenuated. There are some artefacts on the detection side of the sample, minimally compromising the image contrast. In the x -direction the defect is broader than the actual defect size. In agreement with theoretical simulations [5], for a sharply delineated shallow defect in transmission the front boundary between the background and the defect is not seen. Detection occurred at the back surface of the sample, thus concealing the front edge of the material. As expected, the front surface of the defect is not seen. The regularization parameter for this set of reconstructions was 10^{-5} . By virtue of the value of this regularization parameter, one assigns the transmission problem as being less ill-defined than the back-scattering one. It was concluded that when a shallow defect in transmission is being reconstructed, a considerable number of artefacts are created at the back surface of the sample, which can be diminished by averaging all respective laser-position reconstructions.

When comparing figures 6 and 7 it is observed that the back-scattering reconstruction is more accurate. None the less, information about the back side of the defect is obtained in transmission that is not acquired in the back-scattering mode. With this in mind, averaging of the back-scattering and transmission modes may be advantageous. Figure 8 is the average of the average reconstructions in back scattering and transmission, in figures 6 and 7, respectively. The overall contrast and location of the image is an average of the two individual reconstructions. The x -centre of the defect becomes equal to the exact value, due to the fact that in back scattering there was a slight shift in the negative direction from the centre, while in transmission there was a slight shift in the positive direction. In this image, both the back and front surface of the defect are seen. Apart from the defect being

broadened in the x -direction, this is a good reconstruction. One set-back of the composite averaging is that the transmission image brings with it some (minimal) artefacts created at the back surface of the sample, which are not present in the back-scattering image.

The next reconstruction was of the transmission mode experiment number 3, with a hole at the middle of the sampling area. Figure 9 is the average reconstruction of five individual reconstructions at $x_l = 0, 0.75, 1.75, 2.5$ and 3 mm. The regularization parameter for this set of experimental reconstructions was 10^{-5} , prescribing the same ill-conditioning as in the shallow-defect transmission reconstructions. The overall contrast of the defect is -0.45 . The back surface of the defect is reconstructed well and the front surface is mostly reconstructed at the side of the defect where the thermal wave first encounters it. There is a well resolved shape contour of the front boundary of the hole, on the side of the defect that is first encountered by the thermal wave. The back boundary of the defect is reconstructed at $y = 1.5$ mm instead of $y = 1.4$ mm. This can be attributed to the rough grid size chosen. A finer grid in the transmission mode would place the back of the defect at the correct location. The x -location of the defect is exact. Therefore, it was concluded that a defect in the middle of the reconstruction region is reconstructed well at its back boundary, which is independent of the laser position. A draw-back of the individual reconstructions is a strong artefact that is created along the distance between the laser positions and the defect. The front boundary of the defect is reconstructed well along the line of the first encounter between the laser and the defect. For this reason, averaging of multiple laser positions proves to be essential and adequate.

The last experiment reconstructed was number 4. Figure 10 is the average of five individual reconstructions at $x_f = 0, 0.75, 1.5, 2.25$ and 3 mm. The regularization parameter for this set of experimental reconstructions was 10^{-6} , categorizing the problem as less ill-

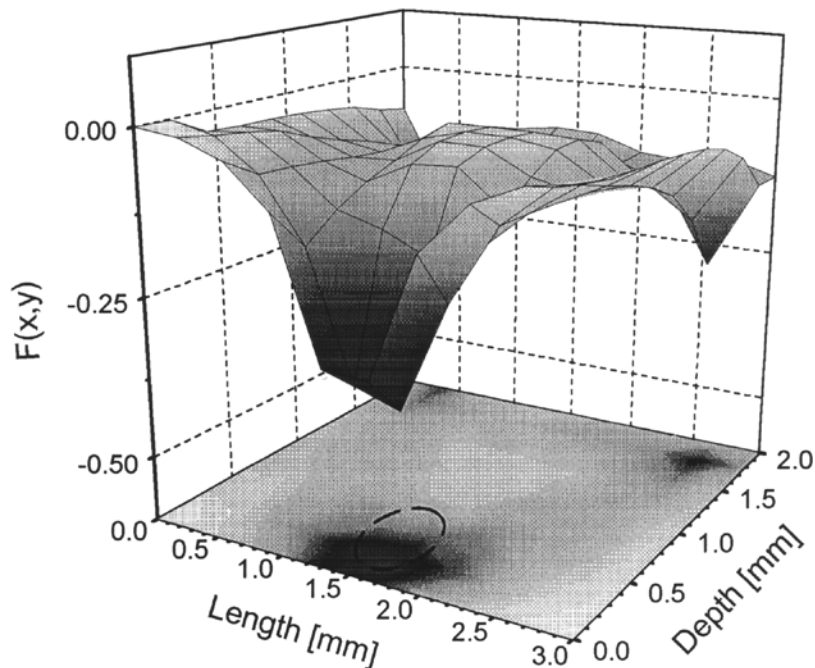


Figure 7. The inverse process-TSDT transmission reconstruction of the shallow defect. An average of five laser positions (true defect shown by the broken circle).

defined than the preceding one. The contrast and location of the defect are accurate. The resulting image is satisfactory. The main disadvantage of this reconstruction is the fact that the image appears broader than the real defect. Also, in agreement to the previous results, the defect is reconstructed well at its back boundary whereas the front of the defect boundary is reconstructed well only on the side of the laser position. Averaging of multiple laser positions improves the reconstruction.

3.3. Problems associated with TSDT

For defect location, most of the error that occurred was related to the y -direction localization. This error occurred because the lateral extent of the scans contributing to reconstruction information was limited. Information obtained from a reconstruction generally depends on the laser position. A defect is delineated accurately on the side closer to the laser position, regardless of which mode of detection is used. The experimental technique of obtaining the surface field is limited to information obtained from the front or back of the sample. A scan along the full perimeter of a cross section would result in obtaining more accurate information about the reconstructed cross section.

In all the reconstructions performed the reconstructed defect was broader in the x -direction. Even though averaging of reconstructions reduced some of the broadening, this factor produced the largest accumulation of error for a reconstruction. This broadening can be attributed to the limited resolution of the experimental detection scheme used to calculate the total surface thermal-wave signal. The experimental field measured was broader than the theoretical one [5].

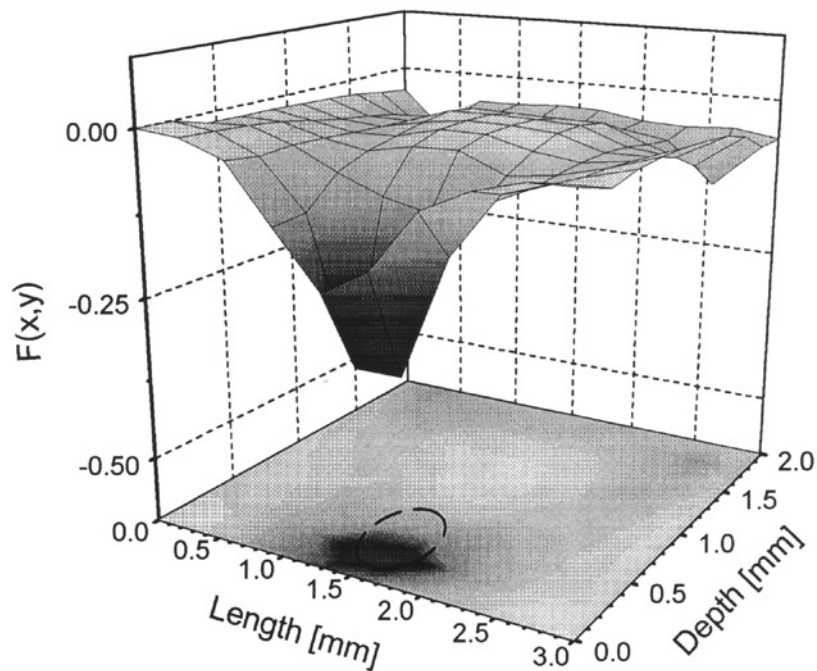


Figure 8. The inverse process-TSDT average reconstruction of back-scattering and transmission-average reconstructions, taken from figures 6 and 7 respectively (true defect shown by the broken circle).

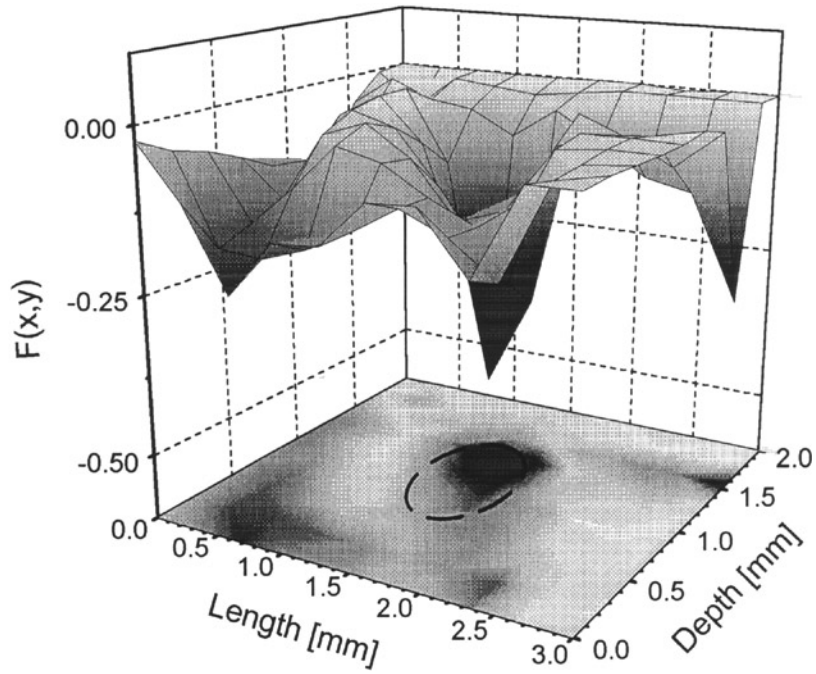


Figure 9. The inverse process-TSDT transmission reconstruction of the middle defect. An average of five laser positions (true defect shown by the broken circle).

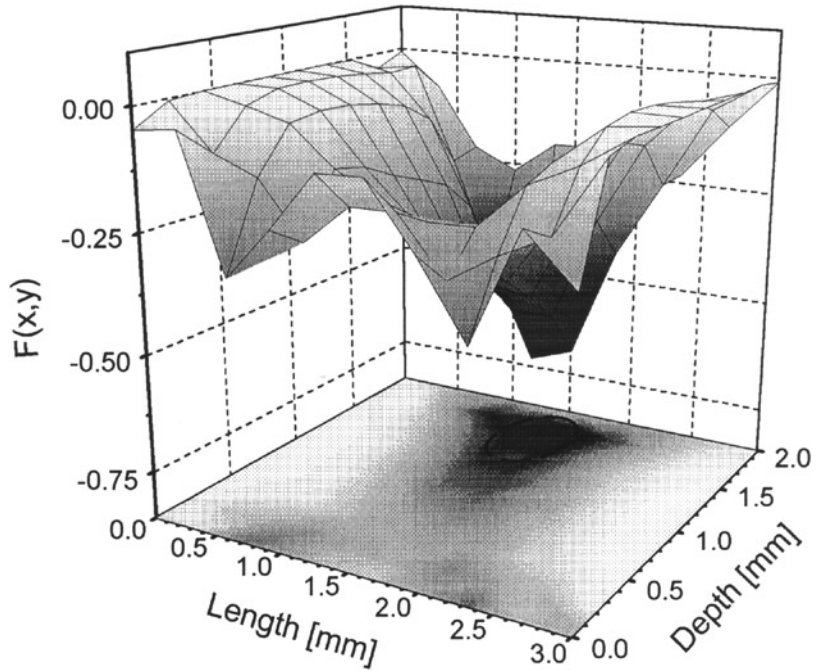


Figure 10. The inverse process-TSDT transmission reconstruction of the deep defect. An average of five laser positions (true defect shown by the broken circle).

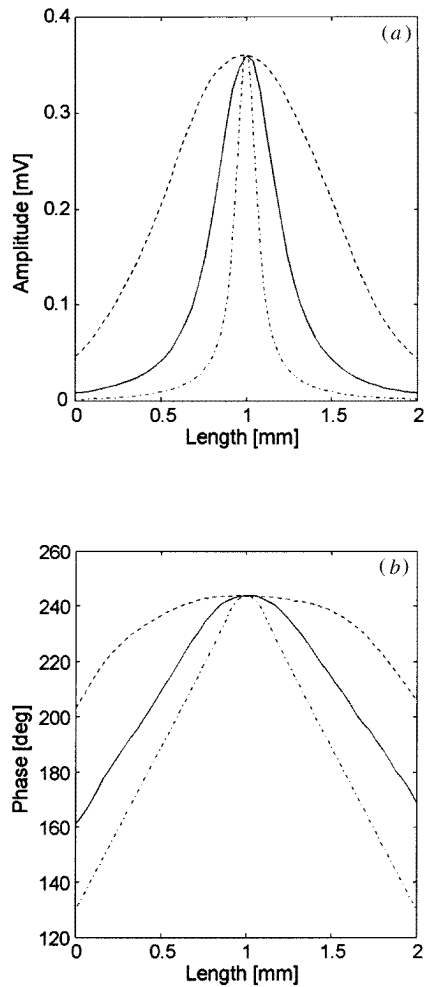


Figure 11. The homogeneous field-steel sample; laser position $x_f = 1$ mm, $f = 15$ Hz; full curve, detector of $50 \mu\text{m}$ aperture; broken curve, detector of 1 mm aperture; chain curve, theoretical field. (a) Amplitude, (b) phase.

Originally, the infrared HgCdTe detector of the experimental system described in section 2, had an active area of $1 \text{ mm} \times 1 \text{ mm}$. Experimental results obtained from cross sectional scanning were very broad as compared with the theoretical homogeneous field [5]. For this reason, that detector was replaced with one with an active square aperture of $50 \mu\text{m} \times 50 \mu\text{m}$. All experiments, for the numerical reconstructions, were performed with this detector, with some loss of signal-to-noise ratio. The effect that the aperture of the detector has on amplitude and phase can be seen in figure 11. The field was measured on a homogeneous mild-steel sample by both HgCdTe detectors. The broken curve represents the HgCdTe detector of 1 mm aperture, and the full curve represents the HgCdTe detector of $50 \mu\text{m}$ aperture. It can be clearly seen that the larger aperture detector broadens the field substantially. The chain curve represents the theoretical back-scattering homogeneous field developed previously [5], with a laser-beam size of $35 \mu\text{m}$ and zero aperture-size broadening. A deconvolution function that removes the broadening of the experimental data should be used. This would diminish any artificial broadening created by the detector, and it would approximate the experimental field to the theoretical one. Work is currently in progress to identify an optimal deconvolution function.

4. Conclusions

In conclusion, averaging of reconstructions of multiple scans leads to an optimal reconstruction of the defect, in both back-scattering and transmission mode. A defect is delineated accurately on the side closer to the laser position, regardless of which mode of detection is used. In back-scattering mode, more information is obtained about the front boundary of the defect. In transmission mode, the back surface of the defect is reconstructed more accurately. In agreement with theoretical computer-simulated findings [5], a shallow defect is reconstructed better in back scattering than in transmission. Additional information obtained for a shallow defect, from a transmission reconstruction, can be used to improve an image. Averaging of a back-scattering and transmission reconstruction was successful in obtaining a better reconstruction. When the experimental back-scattering mode is limited in obtaining information for deeper defects, the transmission mode may be used to advantage. A scan along the perimeter of a cross section, if possible, would result in more accurate information about the reconstructed cross section. The effect of experimental data broadening due to the detection instrumentation should be removed via deconvolution, to further improve the resolution of the TSDT technique.

In general, a dependable method for TSDT was developed. There are still several aspects that have to be researched in order to make TSDT an accepted diffraction tomographic technique for non-destructive testing. The implication of this work, besides establishing a reliable experimental foundation of TSDT, is quite broad in that it has the potential to address several other fields of tomographic science where strong dispersive attenuation presents a reconstruction problem, including medical diffuse photon tomography, attenuated acoustical imaging, and geophysical tomography.

Acknowledgments

The support of the Natural Sciences and Engineering Research Council of Canada (NSERC) and of the Manufacturing Research Corporation of Ontario (MRCO) is gratefully acknowledged.

References

- [1] Munidasa M and Mandelis A 1991 Photopyroelectric thermal-wave tomography of aluminum with ray-optic reconstruction *J. Opt. Soc. Am. A* **8** 1851
- [2] Mandelis A 1991 theory of photothermal wave diffraction tomography via spatial Laplace spectral decomposition *J. Phys. A: Math. Gen.* **24** 2485
- [3] Kak A C and Slaney M 1988 *Principles of Computerized Tomographic Imaging* (New York: IEEE)
- [4] Mandelis A 1995 Green's functions in thermal wave physics: Cartesian coordinate representations *J. Appl. Phys.* **78** 647
- [5] Nicolaidis L and Mandelis A Image-enhanced thermal-wave slice diffraction tomography with numerically simulated reconstructions *Inverse Problems* **13** 1393
- [6] Mandelis A and Mieszkowski M 1990 Thermal wave sub-surface defect imaging and tomography apparatus *US Patent No 4950897*
- [7] Munidasa M, Mandelis A and Ferguson C 1992 Resolution of photothermal tomographic imaging of sub-surface defects in metals with ray-optic reconstruction *Appl. Phys.* **54** 244
- [8] Busse G and Renk K F 1983 Stereoscopic depth analysis by thermal wave transmission for nondestructive evaluation *Appl. Phys. Lett.* **42** 366
- [9] Pade O and Mandelis A 1994 Thermal-wave slice tomography using wave-field reconstruction *Inverse Problems* **10** 185
- [10] Pade O and Mandelis A 1993 Computational thermal-wave slice tomography with backpropagation and transmission reconstructions *Rev. Sci. Instrum.* **64** 3548
- [11] Qian L and Li P 1990 Photothermal radiometry measurement of thermal diffusivity *Appl. Opt.* **29** 4241